Title

Roll-to-Roll Gravure Printed Electrochemical Sensors for Wearable and Medical Devices

Journal

ACS Nano, 12(7)

ISSN

1936-0851

Authors

Bariya, Mallika
Shahpar, Ziba
Park, Hyejin
et al.

Publication Date

2018-07-24

DOI

10.1021/acsnano.8b02505

Peer reviewed

Roll-to-Roll Gravure Printed Electrochemical Sensors for Wearable and Medical Devices

Mallika Bariya[1,2,3*], *Ziba Shahpar*[1,2,3 *], *Hyejin Park*[4], *Junfeng Sun*[4], *Younsu Jung*[4], *Wei Gao*[1,2,3], *Hnin Yin Yin Nyein*[1,2,3], *Tiffany Sun Liaw*[1,2,3], *Li-Chia Tai*[1,2,3], *Quynh P. Ngo* [1,2,3], *Minghan Chao*[1,2,3], *Yingbo Zhao*[1,2,3], *Mark Hettick*[1,2,3], *Gyoujin Cho*[4,‡], *Ali Javey*[1,2,3‡]

[1]Department of Electrical Engineering and Computer Sciences, University of California, Berkeley, California 94720, USA.
[2]Berkeley Sensor and Actuator Center, University of California, Berkeley, California 94720, USA.
[3]Materials Sciences Division, Lawrence Berkeley National Laboratory, Berkeley, California 94720, USA.
[4]Department of Printed Electronics Engineering, Sunchon National University, 255 Jungang-ro, Suncheon, South Korea.
*These authors contributed equally to this work.
‡E-mail: ajavey@berkeley.edu, gcho@scnu.ac.kr

Keywords wearable biosensors, flexible electronics, roll-to-roll processing, gravure printing, multiplexed sensing, *in situ* analysis

Abstract

As recent developments in noninvasive biosensors spearhead the thrust towards personalized health and fitness monitoring, there is a need for high throughput, cost effective fabrication of flexible sensing components. Towards this goal, we present roll-to-roll (R2R) gravure printed electrodes that are robust under a range of electrochemical sensing applications. We use inks and electrode morphologies designed for electrochemical and mechanical stability, achieving devices with uniform redox kinetics printed on 150-meter flexible substrate rolls. We show that these electrodes can be functionalized into consistently high performing sensors for detecting ions,

metabolites, heavy metals, and other small molecules in non-invasively accessed biofluids, including sensors for real-time, *in situ* perspiration monitoring during exercise. This development of robust and versatile R2R gravure printed electrodes represents a key translational step in enabling large-scale, low-cost fabrication of disposable wearable sensors for personalized health monitoring applications.

Wearable biosensors that can probe the body's physiological state at molecular levels have flourished in recent years and show great promise for enabling personalized, point-of-care health and fitness monitoring.[1–13] In particular, advancements in wearable electrochemical sensors have made it possible to non-invasively detect a variety of species including ions, metabolites, acids, heavy metals, and alcohols in biofluids including sweat, saliva, tears, and urine.[4,10,14] Some of the most successful platforms utilize hybrid electronics, combining flexible sensing components that can conformally interface to the body with the high performance and low power advantages of traditional silicon ICs for signal conditioning and transmission.[1–3,5,7,13] For many applications in medical screening or athletic monitoring, it is convenient for the sensing component to be disposable after one-time, on-body use. In this case, sensors of the same type must have consistent performance to ensure that for each new sensing component inserted into the device, minimal calibration is needed to accurately translate the sensor signal into meaningful concentration readings. This minimizes the overhead associated with sensor use, an important practical consideration for promoting wearable prototypes beyond a research setting. Developing high throughput, cost effective methods of fabricating sensing components with high uniformity is therefore critical for the commercial viability of wearable electrochemical devices.

The additive nature and high process speeds of roll-to-roll (R2R) printing technologies offer advantages over traditional methods like photolithography for high throughput fabrication of electronic components on flexible substrates. Of the various available printing techniques, R2R gravure printing shows particular utility as it is intrinsically robust and large-area compatible, making it well suited for industrial-scale production of inexpensive components or devices.[15,16] Further, the simple printing mechanics of R2R gravure allows faster printing speeds with superior resolution and consistency over screen printing, offset printing, or flexography.[15] For these reasons, R2R gravure has previously been developed to print flexible electronic devices including thin film transistors, wireless cyclic voltammetry tags, and a carbon nanotube-based active matrix for tactile sensors, but has been underutilized in the context of recent advancements in wearable electrochemical biosensors.[17–20] Specifically, to advance the wearable sensing platforms that have been proposed in recent years, it is necessary to translate sensor fabrication to high-throughput technologies that deliver consistent device performance across large web lengths while also enabling multiplexed and complex detection mechanisms on the same device. Though gravure printing has been utilized towards biosensor fabrication in the past, there has been limited work on R2R gravure and no assessment of performance variation across large web lengths.[21–24] In contrast to conventional roll-to-plate technologies, R2R gravure involves a moving web under tension and increased shear strain of the doctor blade; printing conditions and inks must be adapted to deposit patterns with fidelity under these harsher conditions. Second, previous works have focused on impedimetric devices that require just two simple metallic electrodes to be printed. To enable a versatile range of amperometric and voltammetric techniques, especially with relatively inexpensive inks, it is necessary to print more complex, multi-layered patterns to realize 3-electrode systems with a stable reference and

conducting yet inert working and counter electrodes. Finally, it is critical to show that these electrodes can be functionalized into sensors that perform reliably *in situ* over extended measurement times. In this work, we refine our ink rheology, printing conditions, and electrode morphologies to address the above points, allowing us to conduct reliable and robust R2R gravure printing of electrochemical electrode arrays on large web lengths with limited performance variation.

We present R2R gravure printed electrodes that can be functionalized into sensors for diverse electrochemical sensing applications (Fig. 1). The electrode arrays realize a canonical 3-electrode system comprising of working, reference, and counter electrodes (Fig. 2), and can be applied towards detecting ions, metabolites, heavy metals, and other small molecules. Large scale, high throughput fabrication on up to 150 meters of flexible substrate makes these electrodes feasible as inexpensive, disposable test strips for medical diagnostics or screening. They are also designed to be compatible with previously demonstrated platforms for *in situ* sweat monitoring, allowing them to be used in wearable sensing applications including continuous tracking of physiological indicators during exercise.[1] The printed electrodes are inert, flexible, and robust under the mechanical strains that accompany on-body use, with consistent electrochemical function that is critical to enabling reliable extraction of physiological data.

Special ink formulation is required to achieve printability under the physical constraints of R2R gravure. An important consequence is that relatively thin layers of ink (up to around 10 μm) are deposited compared to screen printing (up to 100 μm), creating more resistive features.[25] While screen printing allows a thick carbon layer alone to create conductive and inert electrodes, the thin carbon layer deposited by R2R gravure is inadequate. To address this problem, we design a bilayer working electrode morphology comprising of an underlying silver ink layer to

impart conductivity, passivated by an upper carbon layer to achieve an electrochemically inert surface for detection of chemicals or redox processes. Silver ink alone is used for the reference electrode, while an insulating polyethylene resin-based ink is developed to sheathe the exposed electrode wires and prevent crosstalk or shorting in aqueous environments. This modified electrode architecture bridges the gap between requirements for stable electrochemical function and those for good printability using R2R gravure.

We design electrodes with millimeter-scale dimensions to satisfy three criteria: user comfort, sufficient biofluid access, and compatibility with the R2R gravure system. Millimeter-scale sensors are small enough to be unobtrusive when worn, yet large enough to effectively access sites of biofluid secretion such as sweat glands. On the forehead or arms, sweat gland densities are typically around 1.5 glands/mm^2 and generate several tens of nL/min/gland during exercise.[26] A 3 mm-diameter sensor could thus expect to access a couple μL of fresh sweat every few minutes, representing sufficient fluid volume for stable and near real-time readings. For these reasons and the fact that R2R gravure allows excellent pattern fidelity and throughput for printing millimeter-sized features, we design and evaluate electrodes that are 3 mm, 1.5 mm, and 0.75 mm in diameter with applications including perspiration monitoring in mind.[15] We then select the 1.5 mm electrode for more comprehensive studies of device performance variability.

RESULTS AND DISCUSSION

We tailor ink rheology to combine printability requirements with mechanical and electrochemical robustness. Surface tension, viscosity, and wetting characteristics are considered along with other printing parameters to achieve layers with minimal defects or pinholes (Table S1). Using SEM and profilometer measurements, we establish that the printed silver ink layer is on average 250 nm thick with surface roughness of 20 nm. The carbon layer is 1.3 μm thick with

roughness of 0.5 µm, and the insulation layer is 1.5 µm thick with roughness under 10 nm. The surface roughness of the electrodes is evident in the surface SEM images in Fig. 2(d)-(e) which reveal sub-micron features arising from nanoparticle constituents in the inks. These nanoparticles do not significantly enhance the overall electrode surface area and thus have limited impact on sensing performance.[27–29] Instead, they primarily serve to ensure ink stability and processability.[30,31] The silver layer dominates the electrodes' electrical conductivity, and in final printed form has resistivity of 1.8×10^{-4} Ω·cm, comparable to that of other conductive silver inks used for gravure printing.[32]

The performance of solid-state electrochemical electrodes is highly dependent on the surface properties and state of the active electrode area. Pretreatment steps including thermal and electrochemical procedures are common for activating carbon-based electrodes by removing impurities from the electrode surface and increasing surface sensitivity to redox events.[33] To activate the gravure printed electrode arrays before measurement, we employ an optimized sequence of pretreatments including annealing at 160 °C for 1 hour before electrochemically cleaning *via* cyclic voltammetry (CV) in dilute hydrochloric acid. To investigate how each of these procedures impacts the electrode surface composition, we conduct XPS core level measurements using a monochromatic Al source on representative samples halted at different stages in the pretreatment process. In parallel, we explore these samples' electrochemical sensitivity to the $[Fe(CN_6)]^{4-}/[Fe(CN_6)]^{3-}$ redox couple. Fig. S1 in Supplementary Information summarizes these results to demonstrate the effects of pretreatment on the electrodes' surface composition and electrochemical performance. Fig. S1 (a)-(c) reveal that the sensitivity with which the electrodes can relay redox events is increasingly enhanced over the pretreatment procedures, as indicated by the greater definition of the $[Fe(CN_6)]^{4-}/[Fe(CN_6)]^{3-}$ oxidation and

reduction peaks during CV measurements. Changes in the carbon electrode surface composition during pretreatment include an increase in the ratio of carbon-carbon bonds to carbon-oxygen bonds as demonstrated by their relative C 1s subpeak areas (Fig. S1(d)-(f)). Compositional changes in the oxygen content of the silver electrode surface is less dramatic, as indicated by the relative area ratios of Ag 3d subpeaks (Fig. S1(g)-(i)). Overall, pretreatment serves to enhance electrochemical sensitivity while adjusting surface compositions as solvents and residues from the printing process are thermally and electrochemically removed.

The pretreated electrode arrays demonstrate consistent electrochemical performance across electrode dimensions and throughout the gravure printed roll (Fig. 3). Cyclic voltammetry in a solution of 10 mM potassium ferricyanide ($K_3[Fe(CN)_6]$) is selected to verify the electrodes' ability to evince oxidation and reduction events between the $[Fe(CN_6)]^{4-}/[Fe(CN_6)]^{3-}$ redox couple. Fig. 3(a) shows the CV results for electrodes of varying diameter. Separation between the oxidation and reduction peaks is larger than the Nernstian ideal of 60 mV and increases with electrode surface area. This behavior is common among carbon electrodes, which have historically shown a wide range of peak-to-peak separation.[34–37] It stems from the slower electron transfer kinetics of carbon paste electrodes compared to metallic electrodes, as well as resistive losses through the working electrode stack and surrounding solution. The peak positions are affected by a number of factors including the electrode surface morphology and composition, the pre-treatment process, and uncompensated resistive losses.[34,35,38] In Fig. 3(a), despite the particularly strong cathodic peak, the CV oxidation and reduction peaks are of similar area with respect to the ramped baseline, indicating comparable anodic and cathodic charges. Slight differences in the areas can be ascribed to electrochemical irreversibilities introduced by the electrodes and experimental parameters. However, the peak current scales linearly with electrode

area as expected. Further, the CV response curve has low drift across multiple scan cycles after initial stabilization, indicating a stable sensing system (Fig. 3(b)).

For a more extensive analysis of electrode uniformity, the 1.5 mm-diameter electrode was chosen to compare CV results for electrodes sourced from throughout the printed roll. Specifically, we tested 52 electrode arrays from a 20 m segment of the printed roll; that is, 1 electrode array per unit of the gravure cylinder's full pattern to assess variation between printed units. Two key parameters, reduction peak potential and current, are compared as histograms for the 52 electrodes and show tight distributions with mean peak current of -17.2 ± 1.6 μA and potential of 0.38 ± 0.01 V (Fig. 3(c)-(d)). The low spread in these parameters indicates that the electrodes have uniform properties and performance across large swathes of the printed roll. Overall, the stability and repeatability of the CV measurements highlights the utility of these electrodes for point-of-care applications where reliable sensor performance is paramount.

Biofluids contain a wealth of analytes including electrolytes, metabolites, heavy metals, and other small molecules. Detecting these species requires different methods of functionalizing electrodes to have selective recognition elements, as well as different electrochemical detection schemes. To demonstrate the printed electrodes' suitability for a diverse range of sensing modalities, we functionalize them into sensors for pH, potassium (K^+), sodium (Na^+), glucose, copper (Cu^{2+}), and caffeine. Ion sensing requires electrodeposition of ion-to-electron transducing films and casting of selective membrane layers to preferentially bring the target ion to the electrode surface. Potentiometric detection is employed. Glucose sensor fabrication involves deposition of a mediator layer before casting of enzyme entrapped in a hydrogel, and relies on amperometric detection. Heavy metal sensing combines pre-concentration techniques with square wave stripping voltammetry (SWSV) to detect redox peaks associated with

electrodeposition of the target metal ion. Caffeine sensing uses differential pulse voltammetry (DPV) to similarly detect redox transformations of the target molecule.[39] Fig. 4 shows the results of using these fabrication procedures and detection schemes to create and characterize sensors in buffer solutions of varying analyte concentrations. Across physiologically relevant concentration ranges pertinent to each analyte, the sensors maintain linear calibration curves. Further, good stability during measurement in each concentration indicates high performing devices that are robust under a wide potential range and can be used for a variety of sensing applications, attesting to the quality of the underlying electrodes.

To further characterize performance of sensors fabricated on the R2R printed electrode arrays, we select one type of sensor and extensively probe its robustness under long-term and repeated use. We also assess performance uniformity across a collection of similarly fabricated sensors. For these tests, we use 1.5 mm-diameter electrodes sourced from throughout the printed roll and functionalize them into pH sensors *via* electro-polymerization of polyaniline on the working electrode. Fig. 5(a) shows long-term measurement of a representative pH sensor in a sequence of McIlvaine buffer solutions of varying pH. Near-Nernstian sensitivity of -54.2 mV/pH is preserved over the 45-minute interval with drift magnitude lower than 3.5 mV/hr. Fig. 5(b) demonstrates that the sensor responds consistently when cycled through buffer solutions of varying pH, with signal discrepancies of less than 1 mV between concentration cycles indicating good repeatability of results. Fig. 5(c) depicts a histogram of the sensitivities of 40 pH sensors fabricated on electrodes from throughout the gravure printed roll that collectively show mean sensitivity of -53.8 ± 0.9 mV/pH, while Fig. 5(d) compares their potential response at a single pH to demonstrate baseline variation in their voltage signals. The low spread in sensitivities confirms that one-point calibration is sufficient to convert any one pH sensor's electrical signal

into a meaningful pH measurement, making these sensors simple to use in real-world applications with low preparatory overhead.

Following benchtop characterization in buffer solutions, we demonstrate that the printed electrode-based sensors are equally high performing in biofluids including sweat, urine, and saliva. Na^+ is chosen as the target analyte as its concentration in these biofluids is relevant to assessing kidney disease and heart failure among other health complications, as well as for monitoring electrolyte loss or dehydration during exercise.[1,40–43] Na^+ sensors are fabricated on the printed electrode arrays and characterized using multi-point calibration to determine their concentration-to-potential curve. This information is used to accurately covert the sensor signal to a concentration measurement for the sweat, urine, and saliva samples. The sensor results are compared with inductively coupled plasma spectrometry (ICP-MS), a standard method of measuring ionic content (Table 1). There is good coherence between the sensor and ICP-MS results for all the tested samples and across orders of magnitude of Na^+ concentration. This highlights the reliability of the printed array-based sensors for accurate and wide-range quantification of analytes in diverse biofluids.

To establish the versatility of these sensors for personalized health monitoring, we choose a model application in fitness tracking to exhibit sensor durability over continuous, long-term, *in situ* use. Sweat pH is chosen for monitoring as pH can indicate anaerobic metabolism and muscle fatigue and is thus useful to track continuously during exercise.[44] Fig. 6 shows real-time, on-body monitoring of sweat pH during stationary biking. The printed array-based pH sensor is secured conformally against the subject's arm by a wristband. A thin PDMS wall is included to surround the sensing electrodes, creating a well for sweat to accumulate in to reduce evaporation and prevent abrasion of the sensing layer against skin. The sensor can be connected to a

commercial potentiometer or to custom circuitry that enables wireless data collection and transmission, as demonstrated previously for wearable sweat sensors.[1–3,7] Sweat pH measurement is conducted over a duration of exercise including 6 minutes of warm up followed by 45 minutes of biking at a power of 120 W (Fig. 6(a)). During the first 14 minutes, enough sweat does not fill the PDMS well to impinge on the sensor, so no meaningful pH reading is obtained. Once the well is adequately filled, the sensor starts reading and initially shows a gradual increase in pH reflecting a reduction in lactic acid content consistent with the literature (Fig. 6(b)).[3] Sweat pH is stable for the remaining duration of biking. During the trial, sweat is collected from the subject for *ex situ* testing with a commercial pH meter. The on-body data closely matches the commercial pH meter readings, demonstrating the accuracy of the printed array-based sensors for continuous, real-time measurement of physiological indicators in mechanically rigorous *in situ* environments.

While continuous on-body sensing demonstrates the extent to which these printed electrode-based biosensors can be utilized, they are also appropriate for one-time use in medical screening applications. The high throughput, cost effective production of R2R gravure printed electrodes, combined with their ability to easily interface with signal conditioning devices like custom PCBs, makes them well suited for use as inexpensive, disposable test strips for applications including cystic fibrosis diagnosis or sweat glucose monitoring.[13] Additionally, large-scale production of highly uniform sensors can enable research into the physiological relevance of non-invasively accessed biofluids. Uniformly performing R2R printed electrodes make it viable to conduct the population studies needed to understand how sweat, saliva, urine, or tear biomarkers reflect overall health and fitness. In future, gravure printing can be expanded towards direct printing of functional sensor membranes onto the underlying electrodes. By

improving registration accuracy and resolution, highly scaled microelectrodes could be fabricated to enable implantable devices and *in vivo* sensing.[15] More complex hierarchical structures could also be implemented, including incorporating redox buffers into the electrode stack to improve reproducibility of potentials for calibration-free sensing.[45] Eventually, these sensor fabrication processes could be combined with R2R integration of microfluidics and electronic components to enable high speed, large scale production of entire wearable sensing devices.

CONCLUSION

In summary, we have designed R2R gravure printed electrodes for a diverse range of noninvasive biosensing applications geared towards point-of-care health monitoring and diagnosis. With fine-tuned inks and printed layer stacking, the electrodes show consistent redox kinetics and are high performing under a variety of sensing modalities. They can be functionalized into sensors for analytes including ions, metabolites, and heavy metals, and are suitable both for continuous, *in situ* monitoring of physiological indicators as well as for *ex situ*, single-time measurements for medical screenings. We demonstrate high-throughput fabrication across large swathes of flexible substrate, enabling inexpensive, large-scale production of disposable sensing components for wearable hybrid electronics with a view to making personalized health monitoring at molecular levels accessible to the broader community.

METHODS

Ink Formulation

Electrode inks were formulated to overcome challenges including dissolution of the silver ink in aqueous environment, drift of the functionalized sensors, and delamination of the electrode

layers under the mechanical strains of on-body wear. This involved optimizing binder and solvent content and improving printability of the insulation ink to deposit a thick enough layer to encapsulate the electrode wires and shield them from abrasion during *in situ* use. The final ink compositions that successfully met the stability and printability requirements are detailed here. Raw Ag dispersed solution (TEC-PR-041) purchased from InkTec Co., Ltd. Korea was reformulated to achieve stability in aqueous environments. The viscosity and wetting properties of the Ag ink were optimized by adding polymer binder. Specifically, 2g of PVB (poly(vinyl butyral)) with molecular weight of 272.341 g/mol (Sigma Aldrich) was dissolved in Terpineol (18 g) and used as the PVB solution to adjust viscosity and wetting. By adding 10 wt% of PVB binder solution to the Ag dispersed solution (TEC-PR-041; InkTec Co., Ltd. Korea), the viscosity and surface tension were respectively modified to 100 cp and 31 mN/m and provided the best quality Ag printed electrode. For the carbon working and counter electrodes, carbon ink was printed over the Ag layer using carbon paste (DC-15; Dozen TECH corp., Korea) diluted with ECA (Diethylene glycol monoethyl ether acetate) to achieve a viscosity of 350 cp. Insulating ink to passivate the printed Ag lines was formulated by dissolving 20 g of PE (polyethylene) resin (Daejung Chem. Korea) in 80 mL of ECA to achieve a viscosity of 210 cp and surface tension of 31 mN/m.

R2R Gravure Printing

To print the electrode arrays with layers of silver, carbon, and insulation ink, R2R gravure printing was carried on poly(ethylene terephthalate) (PET) web, 250 mm wide and 100 μm thick with lengths up to 150 m (AH71D, SKC, Korea). For continuous printing, R2R gravure with two printing units (manufactured by I-PEN, Korea) was combined with a custom-made servomechanism system with web tension of 5 ± 0.3 kgF. During the printing process, an overlay

printing registration accuracy of ± 20 μm was maintained under a temperature of 23 ± 2 °C and a humidity of 35 ± 2 %. At the first printing unit, Ag electrodes were printed and dried by passing through a drying chamber (150 °C) for 1 min with a printing speed of 6 m/min. A carbon layer was next printed on top of the printed Ag for the working and counter electrodes, and dried by passing through the drying chamber (150 °C) for 1 min. The printed roll was rewound and the Ag and carbon inks further cured for 3 min by again passing through the 150 °C heating chamber at a speed of 2 m/min. Finally, the insulator layer was printed on the rewound PET roll at the same speed of 6 m/min. The total printing time to complete the 3-layer printing and curing of 150,000 electrodes on 150 m of PET web was about 30 min. A summary of the R2R gravure system parameters for printing the electrode arrays is provided in Supplementary Information Table S1.

Electrode Pretreatment

To improve electrochemical performance, pretreatment is necessary to activate the carbon electrode surface by enhancing electron transfer kinetics.[37] Adjusting the thermal anneal and electrochemical acid pretreatment parameters influence the stability of the electrodes' CV curves, and the final pretreatment conditions reported here provide optimized electrode stability and sensitivity to redox events. To activate the carbon electrodes, pretreatment processing was conducted in 2 stages. First, arrays from the R2R gravure printed roll were annealed at 160 °C for 1 hour and allowed to cool back to room temperature. They were then electrochemically cleaned using cyclic voltammetry (CV) in 0.1 M HCl from 0 to 0.8 V for 10 cycles at 100 mV/s to further remove residues and solvents from the printing process.

Sensor Functionalization

Functionalized sensing layers were deposited or grown on the printed arrays using identical procedures and recipes as detailed in our previous work[1–3]. For the pH sensor, aniline was distilled at a temperature of 100 °C and a vapor pressure of 13 mmHg for purification before use. Polyaniline (PANI) was polymerized and electrodeposited on the working electrode surface with a 0.1 M aniline/1 M H_2SO_4 solution using cyclic voltammetry from −0.2 to 1 V for 25 cycles at 100 mV/s. This is the same procedure as reported previously in the literature.[3] For the sodium sensor, a membrane solution was prepared consisting of Na ionophore X (1% weight by weight, w/w), Na-TFPB (0.55% w/w), PVC (33% w/w), and DOS (65.45% w/w). 100 mg of the membrane cocktail was dissolved in 660 μL of tetrahydrofuran. For the potassium sensor, the membrane solution was composed of valinomycin (2% w/w), NaTPB (0.5%), PVC (32.7% w/w), and DOS (64.7% w/w). 100 mg of the membrane cocktail was dissolved in 350 μL of cyclohexanone. For both sodium and potassium sensors, PEDOT:PSS was chosen as the ion-to-electron transducer to minimize potential drift of the ISEs, and was deposited onto the working electrodes by galvanostatic electrochemical polymerization using a solution of 0.01 M EDOT/0.1 M NaPSS. A constant current of 14 μA (2 mA cm^{-2}) was applied to produce polymerization charges of 10 mC on each electrode. Following PEDOT:PSS growth, 10 μL of the sodium membrane cocktail and 4 μL of the potassium membrane cocktail were deposited onto their respective 3 mm electrodes, with cocktail volume scaled down with area for smaller sensor dimensions. For both sensors, the printed silver electrode was made into a PVB reference using a solution of 79.1 mg PVB and 50 mg of NaCl dissolved int 1 mL methanol, 36.2 mg F127, and 0.2 mg of multiwall carbon nanotubes added to minimize potential drift. 10 μL of this solution was deposited on the 3 mm Ag reference electrode but scaled with area for smaller sensor sizes. This is the same procedure as reported previously in the literature for functionalizing ion-

selective electrodes.[1] For the glucose sensor membrane solution, 1% chitosan solution with 2% acetic acid was prepared under magnetic stirring. This membrane solution was combined with glucose oxidase solution (1 mg enzyme in 100 μL of PBS of pH 7.2) in a 1:1 v/v ratio. Prussian Blue mediator was deposited onto the carbon working electrode using cyclic voltammetry from 0 to 0.5 V with respect to the printed Ag reference for one cycle at 20 mV/s, using a plating solution of 2.5 mM $FeCl_3$, 100 mM KCl, 2.5 mM $K_3[Fe(CN)_6]$, and 100 mM HCl. 3 μL of the membrane solution was cast over the 3 mm electrodes and allowed to dry overnight at ambient temperature. Membrane solution volume was scaled with electrode area for smaller electrode dimensions. This is the same procedure as reported previously in the literature.[1] Copper sensors were realized by directly using the pretreated electrodes. Pre-concentration was conducted at -0.2 V for 30 seconds to accumulate copper onto the electrode, followed by square wave stripping voltammetry (SWSV) for detection, as reported previously.[2] Caffeine sensors were prepared by casting 0.8 μL of 0.01% multiwall carbon nanotubes in ethanol, followed by 0.8 μL of 0.01% Nafion, on the pre-treated electrodes as reported previously in the literature.[39]

On-Body Measurement During Exercise

On-body sensor measurement during stationary biking was conducted at the University of California, Berkeley in compliance with human research protocol (CPHS 2014-08-6636) approved by the Berkeley Institutional Review Board (IRB). All subjects gave written, informed consent. An electronically braked leg-cycle ergometer (Kettler E3 Upright Ergometer Exercise Bike) was used for stationary biking. Subjects' wrists were cleaned with water and dried with gauze before securing the sensing patch.

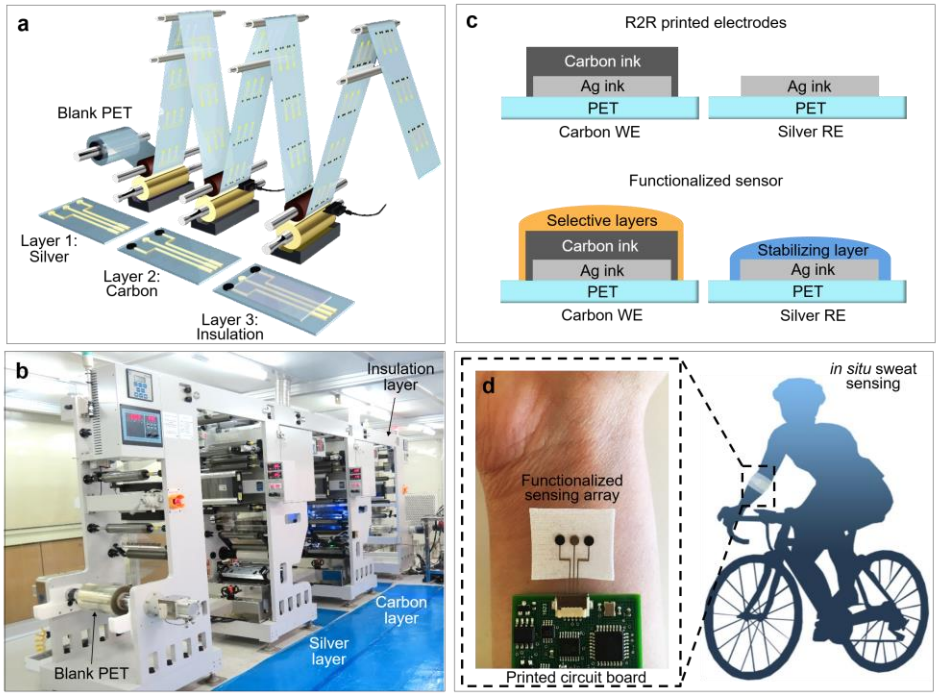

Figure 1. a) Roll-to-roll gravure printing of biocompatible electrode arrays on flexible PET substrate allows high throughput, low cost production of sensing electrodes that can be fabricated with controllable size and density. To print electrode arrays, 3 layers of ink are deposited including silver, carbon, and insulation layers. b) Image of the R2R gravure printing system with modular units for each layer labeled. c) Cross-section schematics of the gravure printed carbon and silver electrodes after printing and then after functionalization. Membranes to selectively target analytes are deposited over the working electrode (WE), while the silver electrode can also be modified to achieve a stable reference (RE). d) Gravure printed electrodes can be functionalized into sensors for *in situ* sensing applications such as continuous, real-time monitoring of analyte profiles in sweat. Sensors can be integrated with custom printed circuit boards for on-site signal processing and transmission, and the whole device worn as a 'smart' wristband during exercise for easy access to sweat.

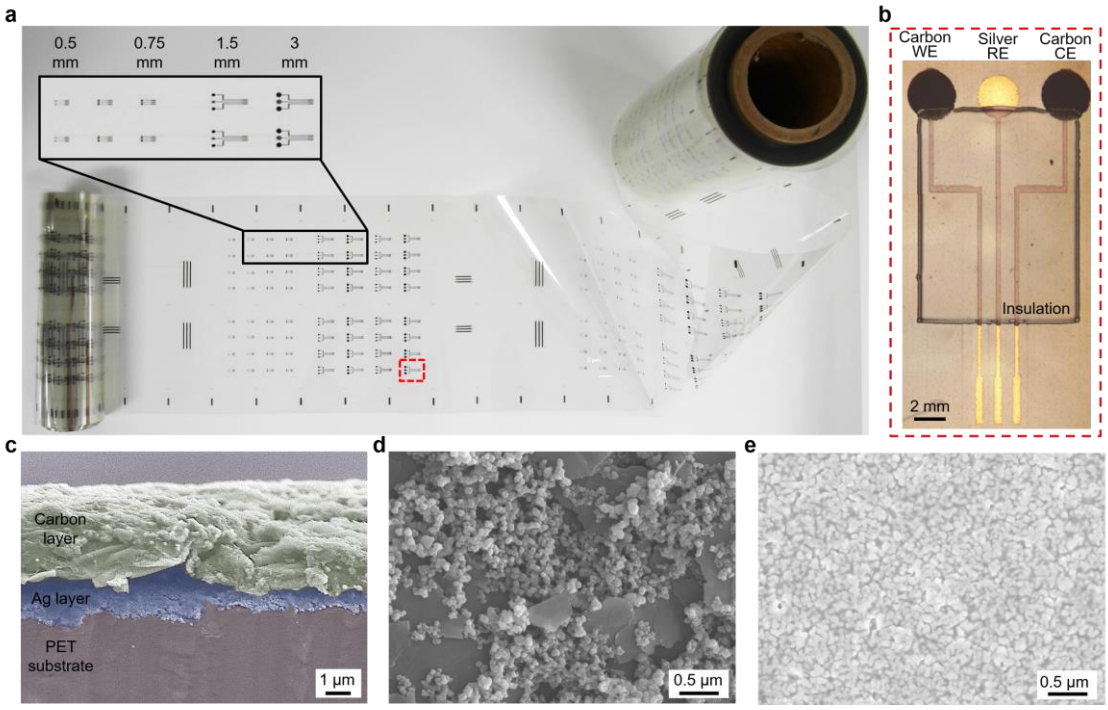

Figure 2. a) Roll-to-roll gravure printed electrodes on a 150-meter roll of PET substrate, with inset showing electrodes ranging from 3 mm down to 0.5 mm in diameter. Electrode array outlined in red is magnified in the subsequent panel. b) Optical micrograph of an array with 3 mm-diameter electrodes showing carbon working electrode, silver reference electrode, carbon counter electrode, and insulation layer. c) False color SEM of the carbon working electrode cross-section shows the hierarchical arrangement of carbon ink (colored yellow) over silver ink (colored blue) on PET substrate. Slight distortion of layer edges is an artefact of cutting for cross-section exposure. d) SEM of carbon electrode surface, and e) SEM of silver electrode surface show nanostructured ink components.

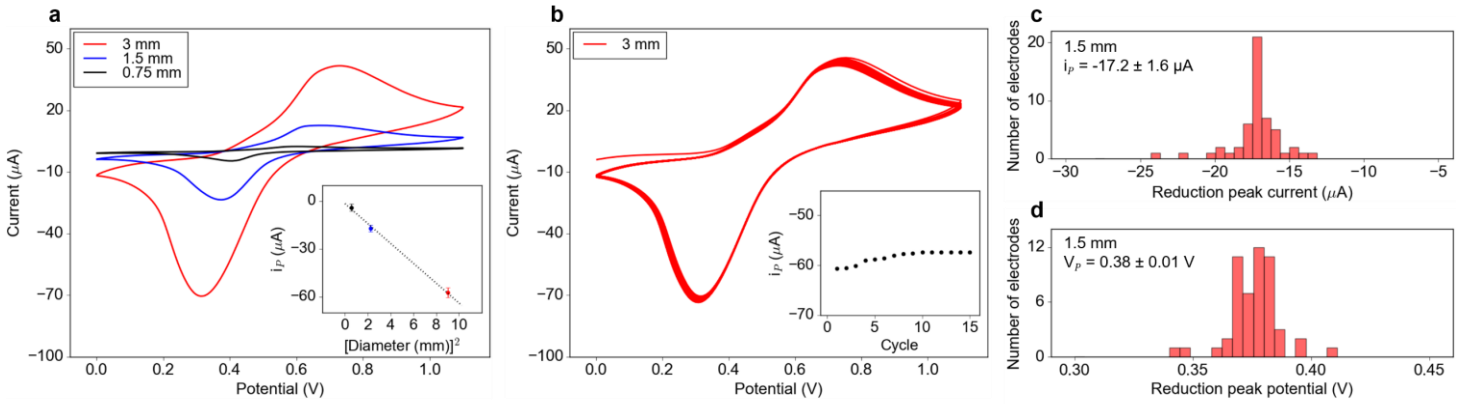

Figure 3. a) Cyclic voltammograms (CV) of 3 mm, 1.5 mm, and 0.75 mm-diameter gravure printed electrodes in 10 mM $K_3[Fe(CN)_6]$. Carbon electrodes constitute the working and counter, while the silver electrode acts as a reference. Inset: Reduction peak current i_P *versus* electrode diameter squared demonstrates a linear relation between the signal and electrode surface area, confirming consistent performance across electrode dimensions. CV response of 5 electrodes of each diameter are averaged for this curve, with standard deviations in i_P of 2.2, 2.0, and 3.1 μA for the 0.75 mm, 1.5 mm, and 3 mm electrodes respectively. b) Multi-cycle CV of a 3 mm electrode array demonstrates good stability, with each scan giving nearly identical current characteristics after initial stabilization. Inset: Reduction peak current is compared across cycles, with drift less than 0.2 μA between cycles. c) CV performance of a collection of 52 1.5 mm-diameter electrode arrays from throughout the printed roll are compared as histograms. Variations in (c) reduction peak current and (d) reduction peak potential are low, indicating uniform electrode quality across large swathes of the printed roll.

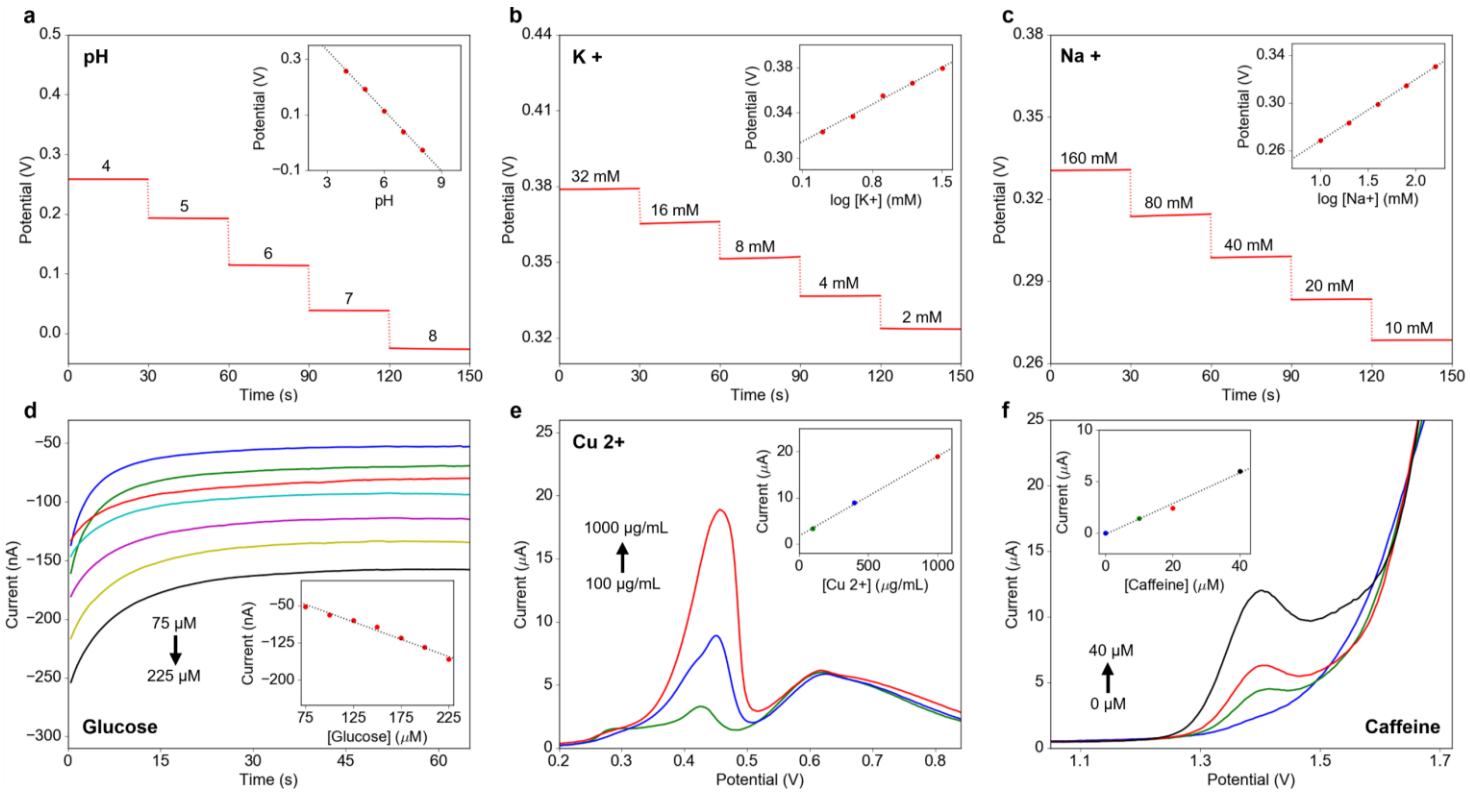

Figure 4. R2R gravure printed electrodes functionalized into different sensors are tested in varying concentrations of their target analytes; the resulting calibration curves are depicted in the insets. a) pH sensor, b) potassium (K^+) sensor, c) sodium (Na^+) sensor, d) glucose sensor, e) copper (Cu^{2+}) sensor, and f) caffeine sensor. Between concentration changes, 30 seconds of rest time are allowed for stabilization.

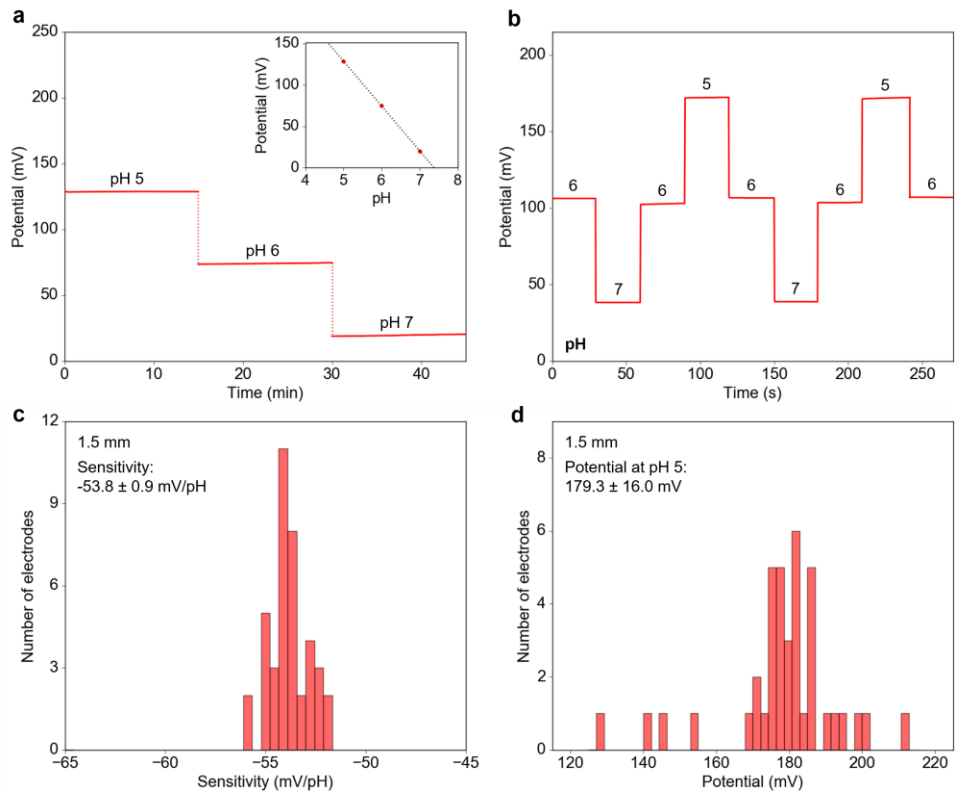

Figure 5. The pH sensor is chosen for extensive analysis of sensor performance and uniformity on the R2R printed electrodes. a) pH sensor is immersed in a sequence of buffer solutions of different pH and measured in each for 15 minutes. The sensor shows good stability with low drift over long-term measurement, with maintained near-Nernstian sensitivity. b) The sensor is cycled through solutions of pH 5, 6, and 7 and shows consistent signal for each pH, demonstrating repeatability. c) A collection of 40 pH sensors are fabricated and their sensitivities measured using calibration solutions of pH 5, 6, and 7. With a mean sensitivity of -53.8 ± 0.9 mV/pH, the printed electrode-based pH sensors show high uniformity in sensitivity with near-Nernstian performance. d) Potential values returned by the 40 pH sensors in a solution of pH 5 are compared as a histogram. Standard deviation of 16.0 mV implies that one-point calibration is necessary for obtaining accurate sensor measurements.

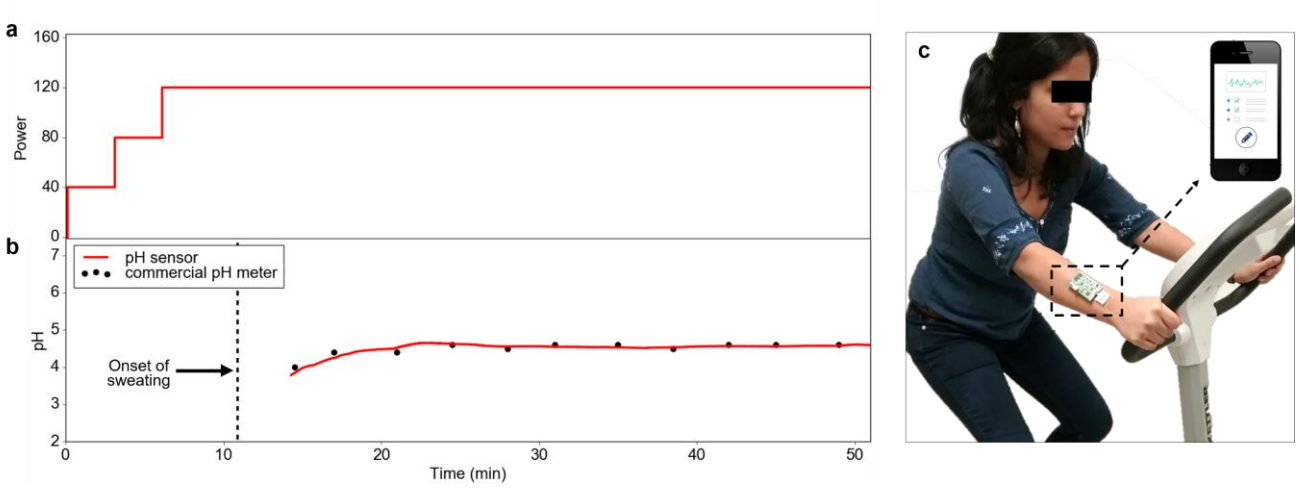

Figure 6. Real time, *in situ* measurement of sweat pH using a R2R gravure printed electrode-based sensor worn on the arm during stationary biking. a) Cycling power is gradually ramped up at the start of the trial and then maintained. b) Real-time sweat pH measurement shows an initial gradual increase and then is stable for the remainder of exercise, consistent with *ex situ* measurements of collected sweat samples using a commercial pH meter. Sweating begins 11 minutes into biking, but no sensor reading is shown for the first 14 minutes as accumulated sweat is too little for the sensor to give a meaningful response. c) Continuous pH analysis is enabled by configuring the sensor array with a custom PCB for signal processing and wireless transmission to a smart phone.

Biosample	Measured [Na^+] (mM)	
	Na^+ Sensor	ICP-MS
Sweat 1	101.2	101.8
Sweat 2	65.2	65.2
Urine 1	137.6	137.4
Urine 2	109.3	110.4
Saliva 1	11.8	11.9
Saliva 2	4.7	5.0

Table 1. Collected biofluid samples tested *ex situ* for sodium content using a R2R printed electrode-based Na^+ sensor *versus* inductively coupled plasma spectrometry (ICP-MS). The sensor measurements cohere with ICP-MS results for sweat, urine, and saliva samples across a wide concentration range. For ICP-MS, samples were diluted before measurement and the resulting concentration signals appropriately compensated. The Na^+ sensor was characterized beforehand *via* multi-point calibration to convert the voltage signal into a concentration measurement.

AUTHOR INFORMATION

Corresponding Authors

‡E-mail: ajavey@berkeley.edu, gcho@scnu.ac.kr

Author Contributions

*These authors contributed equally to this work.

Notes

The authors declare no competing financial interest.

ACKNOWLEDGEMENT

This work in the University of California, Berkeley was supported by NSF Nanomanufacturing Systems for Mobile Computing and Energy Technologies (NASCENT) Center and the Berkeley Sensor & Actuator Center (BSAC). Parts of the device processing and characterization were performed in the Electronic Materials (EMAT) Laboratory funded by the Director, Office of Science, Office of Basic Energy Sciences, Material Sciences and Engineering Division of the US Department of Energy under Contract DE-AC02-05CH11231. G.C. acknowledges supports by a grant (16163KKMFDS001) from the Ministry of Food and Drug Safety in the Republic of Korea (2016). SEM at the Molecular Foundry was supported by the Office of Science, Office of Basic Energy Sciences, of the U.S. Department of Energy under Contract No. DE-AC02-05CH11231. XPS characterization was performed at the Joint Center for Artificial Photosynthesis, supported through the Office of Science of the US Department of Energy under Award Number DE-SC0004993.

References

(1) Gao, W.; Emaminejad, S.; Nyein, H. Y. Y.; Challa, S.; Chen, K.; Peck, A.; Fahad, H. M.; Ota, H.; Shiraki, H.; Kiriya, D.; Lien, D.-H.; Brooks, G. A.; Davis, R. W.; Javey, A. Fully Integrated Wearable Sensor Arrays for Multiplexed *In Situ* Perspiration Analysis. *Nature* **2016**, *529*, 509-514.

(2) Gao, W.; Nyein, H. Y. Y.; Shahpar, Z.; Fahad, H. M.; Chen, K.; Emaminejad, S.; Gao, Y.; Tai, L.-C.; Ota, H.; Wu, E.; Bullock, J.; Zeng, Y.; Lien, D.-H.; Javey, A. Wearable Microsensor Array for Multiplexed Heavy Metal Monitoring of Body Fluids. *ACS Sens*. **2016**, *1*, 866-874.

(3) Nyein, H. Y. Y.; Gao, W.; Shahpar, Z.; Emaminejad, S.; Challa, S.; Chen, K.; Fahad, H. M.; Tai, L.-C.; Ota, H.; Davis, R. W.; Javey, A. A Wearable Electrochemical Platform for Noninvasive Simultaneous Monitoring of Ca^{2+} and pH. *ACS Nano* **2016**, *10*, 7216-7224.

(4) Bariya, M.; Nyein, H. Y. Y.; Javey, A. Wearable Sweat Sensors. *Nat. Electron.* **2018**, *1*, 160–171.

(5) Rose, D. P.; Ratterman, M. E.; Griffin, D. K.; Hou, L.; Kelley-Loughnane, N.; Naik, R. R.; Hagen, J. A.; Papautsky, I.; Heikenfeld, J. C. Adhesive RFID Sensor Patch for Monitoring of Sweat Electrolytes. *IEEE Trans. Biomed. Eng.* **2015**, *62*, 1457–1465.

(6) Choi, J.; Kang, D.; Han, S.; Kim, S. B.; Rogers, J. A. Thin, Soft, Skin-Mounted Microfluidic Networks with Capillary Bursting Valves for Chrono-Sampling of Sweat. *Adv. Healthc. Mater.* **2017**, *6*, 1601355. DOI: 10.1002/adhm.201601355

(7) Kim, J.; Jeerapan, I.; Imani, S.; Cho, T. N.; Bandodkar, A.; Cinti, S.; Mercier, P. P.; Wang, J. Noninvasive Alcohol Monitoring Using a Wearable Tattoo-Based Iontophoretic-Biosensing System. *ACS Sens.* **2016**, *1*, 1011-1019.

(8) Jia, W.; Bandodkar, A. J.; Valdés-Ramírez, G.; Windmiller, J. R.; Yang, Z.; Ramírez, J.; Chan, G.; Wang, J. Electrochemical Tattoo Biosensors for Real-Time Noninvasive Lactate Monitoring in Human Perspiration. *Anal. Chem.* **2013**, *85,* 6553-6560.

(9) Bandodkar, A. J.; Jia, W.; Yardımcı, C.; Wang, X.; Ramirez, J.; Wang, J. Tattoo-Based Noninvasive Glucose Monitoring: A Proof-of-Concept Study. *Anal. Chem.* **2014**, *87*, 394-398.

(10) Bandodkar, A. J.; Wang, J. Non-Invasive Wearable Electrochemical Sensors: A Review. *Trends Biotechnol.* **2014**, *32*, 363–371.

(11) Sonner, Z.; Wilder, E.; Gaillard, T.; Kasting, G.; Heikenfeld, J. Integrated Sudomotor Axon Reflex Sweat Stimulation for Continuous Sweat Analyte Analysis with Individuals at Rest. *Lab. Chip* **2017**, *17*, 2550–2560.

(12) Kim, J.; Imani, S.; Araujo, W. R. de; Warchall, J.; Valdés-Ramírez, G.; Paixão, T. R. L. C.; Mercier, P. P.; Wang, J. Wearable Salivary Uric Acid Mouthguard Biosensor with Integrated Wireless Electronics. *Biosens. Bioelectron.* **2015**, *74*, 1061-1068.

(13) Emaminejad, S.; Gao, W.; Wu, E.; Davies, Z. A.; Nyein, H. Y. Y.; Challa, S.; Ryan, S. P.; Fahad, H. M.; Chen, K.; Shahpar, Z.; Talebi, S.*;* Milla, C.; Javey, A. Autonomous Sweat Extraction and Analysis Applied to Cystic Fibrosis and Glucose Monitoring Using a Fully Integrated Wearable Platform. *Proc. Natl. Acad. Sci.* **2017**, *114*, 4625–4630.

(14) Bandodkar, A. J.; Jeerapan, I.; Wang, J. Wearable Chemical Sensors: Present Challenges and Future Prospects. *ACS Sens.* **2016**, *1*, 464–482.

(15) Grau, G.; Cen, J.; Kang, H.; Kitsomboonloha, R.; Scheideler, W. J.; Subramanian, V. Gravure-Printed Electronics: Recent Progress in Tooling Development, Understanding of

Printing Physics, and Realization of Printed Devices. *Flex. Print. Electron.* **2016**, *1*, 023002. DOI:10.1088/2058-8585/1/2/023002

(16) Abbel, R.; Meinders, E. R. Printing Technologies for Nanomaterials. In *Nanomaterials for 2D and 3D Printing*; Shlomogdassi, Kamyshny, A., Eds.; Wiley-VCH Verlag GmbH & Co. KGaA, 2017; pp 1–26.

(17) Jung, Y.; Park, H.; Park, J.-A.; Noh, J.; Choi, Y.; Jung, M.; Jung, K.; Pyo, M.; Chen, K.; Javey, A.; Cho, G. Fully Printed Flexible and Disposable Wireless Cyclic Voltammetry Tag. *Sci. Rep.* **2015**, *5*, 8105. DOI: 10.1038/srep08105

(18) Lau, P. H.; Takei, K.; Wang, C.; Ju, Y.; Kim, J.; Yu, Z.; Takahashi, T.; Cho, G.; Javey, A. Fully Printed, High Performance Carbon Nanotube Thin-Film Transistors on Flexible Substrates. *Nano Lett.* **2013**, *13*, 3864–3869.

(19) Lee, W.; Koo, H.; Sun, J.; Noh, J.; Kwon, K.-S.; Yeom, C.; Choi, Y.; Chen, K.; Javey, A.; Cho, G. A Fully Roll-to-Roll Gravure-Printed Carbon Nanotube-Based Active Matrix for Multi-Touch Sensors. *Sci. Rep.* **2015**, *5*, 17707. DOI: 10.1038/srep17707

(20) Yeom, C.; Chen, K.; Kiriya, D.; Yu, Z.; Cho, G.; Javey, A. Large-Area Compliant Tactile Sensors Using Printed Carbon Nanotube Active-Matrix Backplanes. *Adv. Mater.* **2015**, *27*, 1561–1566.

(21) Reddy, A. S. G.; Narakathu, B. B.; Atashbar, M. Z.; Rebros, M.; Rebrosova, E.; Joyce, M. K. Gravure Printed Electrochemical Biosensor. *Procedia Eng.* **2011**, *25*, 956–959.

(22) Pavinatto, F. J.; Paschoal, C. W. A.; Arias, A. C. Printed and Flexible Biosensor for Antioxidants Using Interdigitated Ink-Jetted Electrodes and Gravure-Deposited Active Layer. *Biosens. Bioelectron.* **2015**, *67*, 553–559.

(23) Reddy, A. S. G.; Narakathu, B. B.; Atashbar, M. Z.; Rebros, M.; Hrehorova, E.; Joyce, M. Printed Electrochemical Based Biosensors on Flexible Substrates. In *2010 IEEE Sensors*; 2010; pp 1596–1600.

(24) Narakathu, B. B.; Reddy, S. G. A.; Atashbar, M. Z.; Rebrosova, E.; Rebros, M.; Joyce, M. K. A Novel Gravure Printed Impedance Based Flexible Electrochemical Sensor. In *2011 IEEE Sensors Proceedings*; 2011; pp 577–580.

(25) Blayo, A.; Pineaux, B. Printing Processes and Their Potential for RFID Printing. In *Proceedings of the 2005 Joint Conference on Smart Objects and Ambient Intelligence: Innovative Context-aware Services: Usages and Technologies*; sOc-EUSAI '05; ACM: New York, NY, USA, 2005; pp 27–30.

(26) Heikenfeld, J. Non-invasive Analyte Access and Sensing through Eccrine Sweat: Challenges and Outlook circa 2016. *Electroanalysis* **2016**, *28*, 1242–1249.

(27) Luo, X.; Morrin, A.; Killard, A. J.; Smyth, M. R. Application of Nanoparticles in Electrochemical Sensors and Biosensors. *Electroanalysis* **2006**, *18*, 319–326.

(28) Huang, X.-J.; Choi, Y.-K. Chemical Sensors Based on Nanostructured Materials. *Sens. Actuators B Chem.* **2007**, *122*, 659–671.

(29) Huan, T. N.; Ganesh, T.; Kim, K. S.; Kim, S.; Han, S.-H.; Chung, H. A Three-Dimensional Gold Nanodendrite Network Porous Structure and Its Application for an Electrochemical Sensing. *Biosens. Bioelectron.* **2011**, *27*, 183–186.

(30) Kamyshny, A.; Magdassi, S. Conductive Nanomaterials for Printed Electronics. *Small* **2014**, *10*, 3515–3535.

(31) Jeong, S.; Song, H. C.; Lee, W. W.; Lee, S. S.; Choi, Y.; Son, W.; Kim, E. D.; Paik, C. H.; Oh, S. H.; Ryu, B.-H. Stable Aqueous Based Cu Nanoparticle Ink for Printing Well-

Defined Highly Conductive Features on a Plastic Substrate. *Langmuir* **2011**, *27*, 3144–3149.

(32) Kim, S.; Sung, H. J. Effect of Printing Parameters on Gravure Patterning with Conductive Silver Ink. *J. Micromechanics Microengineering* **2015**, *25*, 045004. DOI:10.1088/0960-1317/25/4/045004

(33) Wang, J. Practical Considerations. In *Analytical Electrochemistry*; John Wiley & Sons, Inc., 2006; pp 115–163.

(34) Valentini, F.; Amine, A.; Orlanducci, S.; Terranova, M. L.; Palleschi, G. Carbon Nanotube Purification: Preparation and Characterization of Carbon Nanotube Paste Electrodes. *Anal. Chem.*, **2003**, *75*, 5413–5421.

(35) Batchelor-McAuley, C.; Kätelhön, E.; Barnes, E. O.; Compton, R. G.; Laborda, E.; Molina, A. Recent Advances in Voltammetry. *ChemistryOpen*, **2015**, *4*, 224–260.

(36) Hu, L.; Peng, X.; Huo, K.; Chen, R.; Fu, J.; Li, Y.; Lee, L. Y. S.; Wong, K.-Y.; Chu, P. K. Dominant Factors Governing the Electron Transfer Kinetics and Electrochemical Biosensing Properties of Carbon Nanofiber Arrays. *ACS Appl. Mater. Interfaces* **2016**, *8*, 28872–28879.

(37) Wightman, R. M.; Deakin, M. R.; Kovach, P. M.; Kuhr, W. G.; Stutts, K. J. Method to Improve Electrochemical Reversibility at Carbon Electrodes. *J. Electrochem. Soc.* **1984**, 1*31*, 1578-1583.

(38) A. Wring, S.; P. Hart, J. Chemically Modified, Carbon-Based Electrodes and Their Application as Electrochemical Sensors for the Analysis of Biologically Important Compounds. A Review. *Analyst* **1992**, *117*, 1215–1229.

(39) Tai, L.-C.; Gao, W.; Chao, M.; Bariya, M.; Ngo, Q. P.; Shahpar, Z.; Nyein, H. Y. Y.; Park, H.; Sun, J.; Jung, Y.; et al. Methylxanthine Drug Monitoring with Wearable Sweat Sensors. *Adv. Mater.* **2018**, *30*, 1707442. DOI: 10.1002/adma.201707442

(40) White, A. G.; Gordon, H.; Leiter, L. Studies in Edema. II. The Effect of Congestive Heart Failure on Saliva Electrolye Concentrations. *J. Clin. Invest.* **1950**, *29*, 1445–1447.

(41) Goldberg, M.; Handler, J. S. Hyponatremia and Renal Wasting of Sodium in Patients with Malfunction of the Central Nervous System. *N. Engl. J. Med.* **1960**, *263*, 1037–1043.

(42) Sant'agnese, P. a. D.; Darling, R. C.; Perera, G. A.; Shea, E. Abnormal Electrolyte Composition of Sweat in Cystic Fibrosis of the Pancreas: Clinical Significance and Relationship to the Disease. *Pediatrics* **1953**, *12*, 549–563.

(43) Maughan, R. J. Fluid and Electrolyte Loss and Replacement in Exercise. *J. Sports Sci.* **1991**, *9*, 117–142.

(44) Patterson, M. J.; Galloway, S. D. R.; Nimmo, M. A. Effect of Induced Metabolic Alkalosis on Sweat Composition in Men. *Acta Physiol. Scand.* **2002**, *174*, 41–46.

(45) Hu, J.; Stein, A.; Bühlmann, P. Rational Design of All-Solid-State Ion-Selective Electrodes and Reference Electrodes. *TrAC Trends Anal. Chem.* **2016**, *76*, 102–114.

TOC:

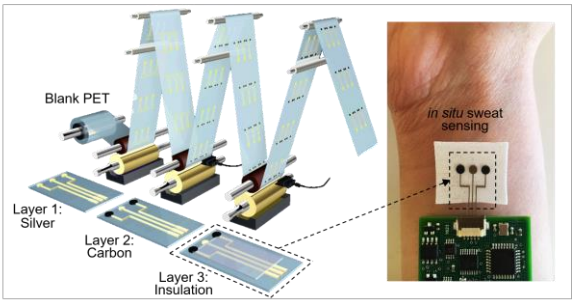
Blank PET
Layer 1:
Silver
Layer 2:
Carbon
Layer 3:
Insulation
in situ sweat
sensing